

Data-Driven Discovery of Conservation Laws from Trajectories via Neural Deflation

Shaoxuan Chen^{*1}, Panayotis G. Kevrekidis¹, Hong-Kun Zhang¹, and Wei Zhu²

¹Department of Mathematics and Statistics, University of Massachusetts Amherst, Amherst, MA 01003-4515, USA

²School of Mathematics, Georgia Institute of Technology, Atlanta, GA 30332, USA

October 10, 2024

Abstract

In an earlier work by a subset of the present authors [1], the method of the so-called neural deflation was introduced towards identifying a complete set of functionally independent conservation laws of a nonlinear dynamical system. Here, we extend by a significant step this proposal. Instead of using the explicit knowledge of the underlying equations of motion, we develop the method directly from system trajectories. This is crucial towards enhancing the practical implementation of the method in scenarios where solely data reflecting discrete snapshots of the system are available. We showcase the results of the method and the number of associated conservation laws obtained in a diverse range of examples including 1D and 2D harmonic oscillators, the Toda lattice, the Fermi-Pasta-Ulam-Tsingou lattice and the Calogero-Moser system.

1 Introduction

The discovery of conservation laws and the potential integrability of dynamical systems are crucial for understanding their evolution and provide valuable insights into their long-term behavior [2]. Identifying conserved quantities is important in a wide range of domains, including optics [3], atomic physics [4], materials science [5], fluid dynamics [6], and plasma physics [7], as it helps to characterize complex phenomena within these areas. Analyzing and uncovering these properties not only illuminates the underlying physical principles but also improves our capacity to model and predict the intricate behaviors of such systems, making this a key focus of ongoing scientific research.

Over the years, numerous theoretical and computational methods have been proposed for identifying the system's integrability [2]. A partial subset of these includes Lax pairs [8], the Painlevé property [9, 10], Lyapunov exponents [11, 12, 13], and Koopman operator theory [14, 15]. Recently, there has been a significant surge of interest in the data-driven discovery of conservation laws and

^{*}Email: shaoxuanchen@umass.edu.

the assessment of system integrability using machine learning; see for some prominent examples, e.g., the works of [16, 17, 18, 19, 20, 21, 22, 1, 23, 24] and the references therein. Despite extensive efforts and advancements in this field, most of these methods still face nontrivial limitations. Many are, in practice, capable of uncovering only a single or a few conservation laws, even for integrable systems, especially so for systems with many degrees of freedom [17, 24]. Methods that purport to discover a comprehensive set of independent conservation laws often either fail in practice or require substantial parameter tuning and human interpretation, reducing their robustness and reliability [16, 18, 20, 21, 22]. Moreover, several approaches necessitate explicit knowledge of the ordinary differential equations (ODEs) governing the dynamics or the precise number of independent conservation laws within the system, thereby limiting their applicability in practical scenarios where only system trajectories may be available in the form of dynamical evolution obtained (or, e.g., experimentally acquired) “data” [21, 22, 1].

Accordingly, in this paper, we propose a data-driven method for discovering a *complete* set of *functionally independent* conservation laws from system trajectories. A key component of our approach is the, so-called, neural deflation technique [1], previously introduced by some of the authors. Unlike the original method, however, our approach does not require explicit knowledge of the underlying ODEs and relies solely on observed system trajectories. This significantly enhances its practicality in real-world scenarios where the exact dynamics are unknown, and only discrete snapshots of the system are available. We demonstrate the effectiveness of our method on widely benchmarked systems, such as the 1D and 2D harmonic oscillators, as well as on integrable and non-integrable differential-difference equation models, including the Toda lattice [25], the Fermi-Pasta-Ulam-Tsingou (FPUT) system [26], the Calogero-Moser model [27, 28], and the discrete sine-Gordon equation [5]. Importantly, we highlight both positive and negative results, illustrating the pitfalls that may arise when working with system trajectories instead of ground-truth ODEs, an aspect that has been, in our view, both underexplored and underreported in previous research.

The rest of the paper is structured as follows. Section 2 discusses related works and their limitations, setting the stage for the present contribution. In Section 3, we provide a brief overview of the theoretical toolbox background on conservation laws, the notion of (Liouville) integrability, Hamiltonian neural networks, and the neural deflation method. Section 4 details our data-driven approach for learning a complete set of conservation laws from system trajectories. In Section 5, we present a series of numerical experiments on various systems, demonstrating the effectiveness of our method and highlighting its potential pitfalls. Finally, we conclude the paper in Section 6 and discuss directions for future work.

2 Related Works

In recent years, there has been a growing focus on using data-driven methods to identify conservation laws and assess system integrability through various machine learning techniques. These approaches fall into two categories: those utilizing explicit knowledge of the underlying ODEs and those relying solely on observed system trajectories.

In the first category, where the underlying ODEs are known, the most recent state-of-the-art

methods are described in [21, 22, 1]. [21] initiated this approach by using a regularized loss function to train a collection of neural networks that parameterize conservation laws, aiming to promote—but not necessarily guarantee—their functional independence. [22] further developed this method by incorporating sparse regression to improve the interpretability of the learned conserved quantities, utilizing a known set of basis functions. Only after a pre-determined set of conservation laws is learned, which are, however, often *neither complete nor functionally independent*, a maximal subset of independent conservation laws is then selected. Consequently, these methods generally cannot ensure that a complete set of independent conservation laws is identified. Indeed, in practical applications to integrable systems, these approaches typically uncover only a few conserved quantities [21], which are argued to be physically relevant. The neural deflation method [1] adopts a different approach by iteratively constructing a sequence of deflated loss functions, ensuring that each newly identified conserved quantity is independent of those found earlier. This method has been shown to successfully discover a complete set of functionally independent conservation laws in various systems. Nonetheless, this method still depends on explicit knowledge of the underlying ODE, and its effectiveness in accurately determining the exact number of conserved quantities based solely on system trajectories remains uncertain.

In the second category, which assumes only the availability of system trajectories, the methods tend to be less robust and reliable, often requiring significant parameter tuning, human interpretation, or additional assumptions. The Siamese neural networks proposed by Wetzel et al. [29] can only learn a single conservation law. While the method proposed by Ha and Jeong [24] can theoretically learn multiple conserved quantities, it requires “grouped data” sampling from level sets of previously identified conserved quantities, which significantly limits its practical applicability. The model-agnostic learning technique by Arora et al. [19] necessitates explicit knowledge of the exact number of independent conservation laws in the system. For manifold learning approaches [18, 20], there is typically no guarantee that the correct dimension of the isosurface of the conserved quantities—and therefore the correct number of conservation laws—will be learned and identified. The aim of the present work is to combine the methodological advantages of [1] with an implementation that can work directly with data.

3 Background and Motivation

This section provides a brief overview of the theoretical notions of interest regarding Hamiltonian systems, their conservation laws, and the method of neural deflation.

3.1 Hamiltonian Systems and Conservation Laws

Consider a *Hamiltonian system* of d degrees of freedom,

$$\frac{d\mathbf{x}}{dt} = \mathbf{f}(\mathbf{x}), \quad \mathbf{f}(\mathbf{x}) = J(\mathbf{x})\nabla H(\mathbf{x}), \quad \forall \mathbf{x} \in D \subset \mathbb{R}^{2d}, \quad (1)$$

where $H : D \rightarrow \mathbb{R}$ is the Hamiltonian function, and $J(\mathbf{x}) \in \mathbb{R}^{2d \times 2d}$ is an antisymmetric matrix. Let F and G be two smooth functions over the phase space D , their *Poisson bracket*, $\{F, G\} : D \rightarrow \mathbb{R}$, is given by

$$\{F, G\}(\mathbf{x}) := \nabla F(\mathbf{x})^T J(\mathbf{x}) \nabla G(\mathbf{x}), \quad \forall \mathbf{x} \in D.$$

In particular, under the canonical coordinates $\mathbf{x} = (\mathbf{q}, \mathbf{p})$, where $\mathbf{q}, \mathbf{p} \in \mathbb{R}^d$ are the generalized positions and conjugate momenta, we have

$$J(\mathbf{x}) \equiv \begin{bmatrix} 0 & I_d \\ -I_d & 0 \end{bmatrix}, \quad \{F, G\} = \nabla_{\mathbf{q}} F \cdot \nabla_{\mathbf{p}} G - \nabla_{\mathbf{p}} F \cdot \nabla_{\mathbf{q}} G,$$

and the familiar Hamilton’s equations are of the form:

$$\begin{cases} \frac{d\mathbf{q}}{dt} = \nabla_{\mathbf{p}} H, \\ \frac{d\mathbf{p}}{dt} = -\nabla_{\mathbf{q}} H. \end{cases} \quad (2)$$

A C^1 smooth function $I : D \rightarrow \mathbb{R}$ is called a *conservation law* of system (1) if it remains constant over system trajectories. That is, for any $\mathbf{x}(t)$ that is a solution of Eq. (1), we have

$$I(\mathbf{x}(t)) \equiv I(\mathbf{x}(0)), \quad \forall t \geq 0.$$

It is easy to verify that I is a conservation law of system (1) if and only if its Poisson bracket with the Hamiltonian H vanishes over D , i.e.,

$$\{I, H\}(\mathbf{x}) = \nabla I(\mathbf{x}) \cdot \mathbf{f}(\mathbf{x}) = 0, \quad \forall \mathbf{x} \in D \quad (3)$$

Let $\{I_k : D \rightarrow \mathbb{R}\}_{k=1}^K$ be a collection of K conservation laws of system (1), we say they are *functionally independent* if their gradients $\{\nabla I_k(\mathbf{x})\}_{k=1}^K$ are linearly independent vectors in \mathbb{R}^{2d} for almost every $\mathbf{x} \in D$. Intuitively, this means there is no non-trivial relationship among these conserved quantities that allows one to be expressed as a (nonlinear) combination of the others. Moreover, these conservation laws are said to be *in involution*, or *Poisson commuting*, if their pairwise Poisson brackets vanish, i.e., $\{I_j, I_k\} = 0, \forall j \neq k$. For a Hamiltonian system with d degrees of freedom, there can be at most d functionally independent conservation laws in involution. When a system admits d such conserved quantities, it is said to be completely integrable in the Liouville sense [30].

3.2 Neural Deflation Method

The neural deflation method [1] provides a systematic, data-driven approach for identifying a maximal set of functionally independent, Poisson-commuting conservation laws when the underlying dynamics, i.e., $\mathbf{f}(\mathbf{x})$ in Eq. (1), is explicitly known. The core idea is to *iteratively* learn each conservation law using a *deflated* loss function, ensuring that each newly identified conserved quantity is both in involution and functionally independent from the previously discovered ones. This approach is inspired by the concept of “deflation”, which is used to find multiple steady states of partial differential equations by adjusting the loss function to discourage solutions that are similar to those already identified [31].

The process begins by randomly sampling a training set \mathcal{T} and a validation set \mathcal{V} from $D \subset \mathbb{R}^{2d}$. Each conserved quantity $I_k(\mathbf{x})$ is parameterized using a neural network $I_k(\mathbf{x}; \boldsymbol{\theta}_k)$, where $\boldsymbol{\theta}_k$ are

the trainable parameters. To learn the first conservation law $I_1(\mathbf{x}; \boldsymbol{\theta}_1)$, the following loss function is minimized, based on the condition (3):

$$\mathcal{L}_1(\boldsymbol{\theta}_1; \mathcal{T}) := \frac{1}{|\mathcal{T}|} \sum_{\mathbf{x} \in \mathcal{T}} \left| \widehat{\mathbf{f}}(\mathbf{x}) \cdot \widehat{\nabla I_1}(\mathbf{x}; \boldsymbol{\theta}_1) \right|^2, \quad (4)$$

where $\widehat{\mathbf{f}}(\mathbf{x})$ and $\widehat{\nabla I_1}(\mathbf{x}; \boldsymbol{\theta}_1)$ are the l^2 -normalized vectors of $\mathbf{f}(\mathbf{x})$ and $\nabla I_1(\mathbf{x}; \boldsymbol{\theta}_1)$, respectively, evaluated on the training set \mathcal{T} . This normalization makes the loss function scale-invariant and prevents learning the trivial conservation law $I_1(\mathbf{x}; \boldsymbol{\theta}_1) \equiv C$.

The process continues by iteratively learning additional conservation laws inductively as follows. Assuming $K - 1$ conserved quantities $\{I_k(\mathbf{x}; \boldsymbol{\theta}_k^*)\}_{k=1}^{K-1}$ have already been found, the K -th conservation law $I_K(\mathbf{x}; \boldsymbol{\theta}_K)$ is trained using the following deflated loss function $\mathcal{L}_K(\boldsymbol{\theta}_K; \mathcal{T})$, while keeping the parameters of the previous networks $\{\boldsymbol{\theta}_k^*\}_{k=1}^{K-1}$ fixed:

$$\mathcal{L}_K(\boldsymbol{\theta}_K; \mathcal{T}) := \frac{1}{|\mathcal{T}|} \sum_{\mathbf{x} \in \mathcal{T}} \frac{\overbrace{\ell_{\text{conserv}}[\boldsymbol{\theta}_K; \mathbf{x}]}^{\text{conservation loss}} + \overbrace{\sum_{k=1}^{K-1} \ell_{\text{inv}}[\boldsymbol{\theta}_k^*, \boldsymbol{\theta}_K; \mathbf{x}]}^{\text{involution loss}}}{\underbrace{K \left| \ell_{\text{ind}}[\boldsymbol{\theta}_K | \boldsymbol{\theta}_1^*, \dots, \boldsymbol{\theta}_{K-1}^*; \mathbf{x}] \right|^\alpha}_{\text{independent loss}}}}, \quad (5)$$

where

- The *conservation loss*, $\ell_{\text{conserv}}[\boldsymbol{\theta}_K; \mathbf{x}]$, ensures that $I_K(\mathbf{x}; \boldsymbol{\theta}_K)$ is indeed a conserved quantity, and is defined similarly to Eq. (4):

$$\ell_{\text{conserv}}[\boldsymbol{\theta}_K; \mathbf{x}] := \frac{1}{|\mathcal{T}|} \sum_{\mathbf{x} \in \mathcal{T}} \left| \widehat{\mathbf{f}}(\mathbf{x}) \cdot \widehat{\nabla I_K}(\mathbf{x}; \boldsymbol{\theta}_K) \right|^2.$$

- The *involution loss*:

$$\ell_{\text{inv}}[\boldsymbol{\theta}_k^*, \boldsymbol{\theta}_K; \mathbf{x}] := |\{I_k(\cdot; \boldsymbol{\theta}_k^*), I_K(\cdot; \boldsymbol{\theta}_K)\}(\mathbf{x})|^2$$

stipulates that $I_K(\cdot; \boldsymbol{\theta}_K)$ is in involution with all previously identified conservation laws $\{I_k(\mathbf{x}; \boldsymbol{\theta}_k^*)\}_{k=1}^{K-1}$.

- The *independent loss* in the deflated denominator is defined as:

$$\ell_{\text{ind}}[\boldsymbol{\theta}_k^* | \boldsymbol{\theta}_1, \dots, \boldsymbol{\theta}_{K-1}; \mathbf{x}] := \left\| \text{Proj}_{\text{span}\{\widehat{\nabla I_k}(\mathbf{x}; \boldsymbol{\theta}_k^*)\}_{k \in [K-1]}^\perp} \widehat{\nabla I_K}(\mathbf{x}; \boldsymbol{\theta}_K) \right\|^2,$$

where $\text{Proj}_{\text{span}\{\widehat{\nabla I_k}(\mathbf{x}; \boldsymbol{\theta}_k^*)\}_{k \in [K-1]}^\perp} \widehat{\nabla I_K}(\mathbf{x}; \boldsymbol{\theta}_K)$ represents the projection of $\widehat{\nabla I_K}(\mathbf{x}; \boldsymbol{\theta}_K)$ onto the orthogonal complement of the subspace spanned by $\{\widehat{\nabla I_k}(\mathbf{x}; \boldsymbol{\theta}_k^*)\}_{k \in [K-1]}$ in \mathbb{R}^{2d} . This term introduces a singularity that penalizes any lack of independence between $\widehat{\nabla I_K}(\mathbf{x}; \boldsymbol{\theta}_K)$ and the previously learned $\{\widehat{\nabla I_k}(\mathbf{x}; \boldsymbol{\theta}_k^*)\}_{k \in [K-1]}$. The deflation parameter $\alpha > 0$ is a hyperparameter that controls the strength of this functional independence constraint between $I_K(\cdot; \boldsymbol{\theta}_K)$ and $\{I_k(\mathbf{x}; \boldsymbol{\theta}_k^*)\}_{k=1}^{K-1}$.

One can easily show that this method is *consistent* in the infinite-sample limit in the following sense: if the previously obtained $\{I_k(\cdot; \boldsymbol{\theta}_k^*)\}_{k=1}^{K-1}$ accurately parameterize a ground-truth set of independent conservation laws in involution, and if the empirical averages over the training set \mathcal{T} are replaced by expectations with respect to an absolutely continuous probability measure, then the loss $I_K(\cdot; \boldsymbol{\theta}_K^*)$ is zero *if and only if* $\{I_k(\cdot; \boldsymbol{\theta}_k^*)\}_{k=1}^K$ forms a new set of K independent Poisson-commuting conservation laws. For more details, see the proof provided in [1].

The process is repeated until a significant increase in the loss function $\mathcal{L}_K(\boldsymbol{\theta}_K^*; \mathcal{V})$ is observed on the validation set \mathcal{V} . At that point, $\{I_k(\cdot; \boldsymbol{\theta}_k^*)\}_{k=1}^{K-1}$ is declared a maximal set of $d_0 = K - 1$ independent conservation laws in involution for the system.

Given the expressiveness of neural networks and the availability of the ground-truth Hamiltonian $H(\mathbf{x})$, it is feasible to sample an extensive training set \mathcal{T} from D to construct the consistent loss (5) for training any conserved quantities. However, the effectiveness of this neural deflation method becomes uncertain when direct access to $H(\mathbf{x})$ is not available, and only a limited set of observed or simulated trajectories can be used. This challenge is the central focus of this work.

4 Method

A natural strategy to address this problem is to infer the Hamiltonian of the system from its observed trajectories. Since the loss functions (4) and (5) do not require a closed-form expression for the Hamiltonian but only the ability to sample sufficient values of the vector field $\mathbf{f}(\mathbf{x}) = J(\mathbf{x})\nabla H(\mathbf{x})$ for $\mathbf{x} \in \mathcal{T} \subset D$, a numerical approximation of the ground-truth Hamiltonian suffices. This approach naturally raises two questions:

- How can we approximate the Hamiltonian using only observed or simulated system trajectories, and what is the expected accuracy of this approximation?
- If we use a numerically approximated Hamiltonian in place of the exact Hamiltonian in the neural deflation method, will the method still function effectively?

4.1 Hamiltonian Neural Network

There is a substantial body of research on data-driven learning of Hamiltonian systems [32, 33, 34, 35, 36, 37, 38, 39, 40, 41]. Among these, the Hamiltonian Neural Network (HNN) [34] stands out as one of the pioneering approaches. Several improvements to HNNs have been proposed, including the use of more accurate integrators [39], enhanced modeling of continuous-time trajectories [42], and adaptation to various bifurcation parameters [35]. In this paper, we will adopt the original HNN [34] to derive a neural network approximation of the Hamiltonian from observed system trajectories. This choice is made both for its simplicity and to facilitate the evaluation of whether a numerically approximated Hamiltonian (with inherent uncertainties) can effectively support the downstream neural deflation learning of the remaining conservation laws.

For simplicity, let us assume that the Hamiltonian system is observed using the canonical coordinates $\mathbf{x} = (\mathbf{q}, \mathbf{p}) \in \mathbb{R}^{2d}$. The dataset consists of a collection of I trajectories. Note that here,

we slightly abuse the notation I , which was previously used with a subscript to denote/index the conservation laws, to also represent the number of trajectories in the data. Each trajectory is sampled at J time steps with a uniform time interval Δt .

$$\mathcal{D} = \left\{ \mathbf{x}^{(i,j)} = \left(\mathbf{q}^{(i,j)}, \mathbf{p}^{(i,j)} \right) : 1 \leq i \leq I, 1 \leq j \leq J \right\}, \quad (6)$$

where $\mathbf{q}^{(i,j)} = (q_1^{(i,j)}, \dots, q_d^{(i,j)}) \in \mathbb{R}^d$ represents the generalized position coordinates, and $\mathbf{p}^{(i,j)} = (p_1^{(i,j)}, \dots, p_d^{(i,j)})$ denotes the conjugate momenta. Here, $i \in \{1, \dots, I\}$ indexes the sampled trajectories, and $j \in \{1, \dots, J\}$ represents the time index within each trajectory.

Assuming a small time interval Δt , one can estimate the time derivative of the observed trajectories using finite differences, yielding the time-derivative dataset:

$$\dot{\mathcal{D}} = \left\{ \dot{\mathbf{x}}^{(i,j)} = \left(\dot{\mathbf{q}}^{(i,j)}, \dot{\mathbf{p}}^{(i,j)} \right) : 1 \leq i \leq I, 1 \leq j \leq J \right\}. \quad (7)$$

For high-accuracy time-derivative approximations, we typically use 8th-order central finite differences. However, experiments show that lower-order approximations, though less precise, generally yield qualitatively similar final outcomes for our method.

We can then parameterize the unknown Hamiltonian $H(\mathbf{q}, \mathbf{p})$ using an HNN, denoted as $H_{\boldsymbol{\xi}}(\mathbf{q}, \mathbf{p})$, where $\boldsymbol{\xi}$ represents the network parameters. The HNN is trained using the following loss function based on the Hamiltonian dynamics (2):

$$\mathcal{L}_{\text{HNN}}(\boldsymbol{\xi}; \mathcal{D}, \dot{\mathcal{D}}) = \frac{1}{IJ} \sum_{i,j} \left\| \nabla_{\mathbf{p}} H_{\boldsymbol{\xi}} \left(\mathbf{q}^{(i,j)}, \mathbf{p}^{(i,j)} \right) - \dot{\mathbf{q}}^{(i,j)} \right\|^2 + \left\| \nabla_{\mathbf{q}} H_{\boldsymbol{\xi}} \left(\mathbf{q}^{(i,j)}, \mathbf{p}^{(i,j)} \right) + \dot{\mathbf{p}}^{(i,j)} \right\|^2, \quad (8)$$

One solves the above problem through optimization, where the gradients $(\nabla_{\mathbf{q}} H_{\boldsymbol{\xi}}, \nabla_{\mathbf{p}} H_{\boldsymbol{\xi}})$ are obtained via automatic differentiation. The resulting minimizer $\boldsymbol{\xi}^*$ provides a parameterized approximation of the Hamiltonian, $H_{\boldsymbol{\xi}^*}(\mathbf{q}, \mathbf{p})$.

4.2 Neural Deflation with HNN

Once the neural network approximation $H_{\boldsymbol{\xi}^*}(\mathbf{q}, \mathbf{p})$ of the Hamiltonian is obtained, it can be incorporated into the neural deflation method described in Section 3.2. This involves replacing the unknown Hamiltonian $H(\mathbf{x})$ and the vector field $\mathbf{f}(\mathbf{x})$ with their numerically approximated counterparts, $H_{\boldsymbol{\xi}^*}(\mathbf{x})$ and $\mathbf{f}_{\boldsymbol{\xi}^*}(\mathbf{x})$, respectively. Our method is summarized in Algorithm 1, with a schematic representation presented in Figure 1.

In practice, $H_{\boldsymbol{\xi}^*}(\mathbf{q}, \mathbf{p})$, the trained HNN, provides only a numerical approximation of the true Hamiltonian $H(\mathbf{q}, \mathbf{p})$, which inevitably introduces inaccuracies, especially in regions of the domain D that are not covered by the sampled trajectories. This work seeks to carefully evaluate these inaccuracies and their effect on the neural deflation learning of the remaining conservation laws.

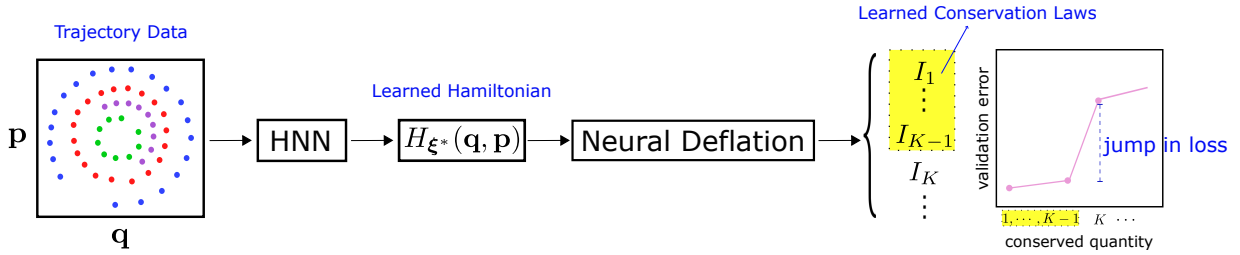


Figure 1: Schematic representation of our method. Trajectory data (with different colors representing distinct trajectories) are first input into the Hamiltonian Neural Network (HNN) to learn the Hamiltonian $H_{\xi^*}(\mathbf{q}, \mathbf{p})$, which is then incorporated into the neural deflation method. A jump in the validation loss at I_K signals the successful learning of $K - 1$ Poisson-commuting, functionally independent conservation laws.

5 Numerical Experiments

In this section, we present the results of our algorithm in learning independent conservation laws from the simulated trajectories of various examples, including the 1D and 2D harmonic oscillators, the discrete sine-Gordon system, the Calogero-Moser system, the integrable Toda lattice, and the nonintegrable Fermi-Pasta-Ulam-Tsingou system.

- **1D and 2D harmonic oscillators.** We assume the *1D harmonic oscillator* to be describing the motion of a mass m attached to a spring with a spring constant k . The relevant canonical coordinates are $\mathbf{x} = (q, p) \in \mathbb{R}^2$, where q is the position and p is the momentum. The equation of motion is given by:

$$\dot{q} = \frac{p}{m}, \quad \dot{p} = -kq.$$

The Hamiltonian for the 1D harmonic oscillator consisting of the sum of kinetic and potential energies reads:

$$H = \frac{p^2}{2m} + \frac{1}{2}kq^2. \quad (9)$$

The *2D harmonic oscillator* generalizes the motion to two dimensions, described by the coordinates $\mathbf{x} = (\mathbf{q}, \mathbf{p})$, where $\mathbf{q} = (q_1, q_2)$ and $\mathbf{p} = (p_1, p_2)$. The corresponding Hamiltonian for the 2D system is:

$$H = \frac{1}{2}k_1q_1^2 + \frac{p_1^2}{2m_1} + \frac{1}{2}k_2q_2^2 + \frac{p_2^2}{2m_2}$$

Both the 1D and 2D harmonic oscillators are simple, integrable systems, making them natural examples for a preliminary assessment of the accuracy of our method. We will use these systems to demonstrate how effectively the HNN can learn the true Hamiltonian from observed trajectories and evaluate its impact on the subsequent neural deflation learning of conservation laws.

Algorithm 1: Neural deflation with HNN

Input: $\mathcal{D} = \{\mathbf{x}^{(i,j)} : 1 \leq i \leq I, 1 \leq j \leq J\} \subset D \subset \mathbb{R}^{2d}$, a collection of I trajectories of a Hamiltonian system, each sampled at J time steps with a uniform time interval Δt .

Output: Neural network approximation $H_{\xi}(\mathbf{x})$ of the Hamiltonian. A maximal set $\{I_k(\cdot; \theta_k^*)\}_{k=1}^{d_0}$ of functionally independent, Poisson-commuting conservation laws.

- 1 Estimate the time-derivatives $\dot{\mathcal{D}} = \{\dot{\mathbf{x}}^{(i,j)} : 1 \leq i \leq I, 1 \leq j \leq J\}$ (7) using finite differences;
 - 2 $\xi^* \leftarrow \arg \min_{\xi} \mathcal{L}_{\text{HNN}}(\xi; \mathcal{D}, \dot{\mathcal{D}})$ given by Eq. (8), and use the trained HNN, $H_{\xi^*}(\mathbf{x})$, as a surrogate Hamiltonian for all subsequent steps;
 - 3 Randomly sample a training set \mathcal{T} and a validation set \mathcal{V} from the phase space $D \subset \mathbb{R}^{2d}$;
 - 4 $\theta_1^* \leftarrow \arg \min_{\theta_1} \mathcal{L}_1(\theta_1; \mathcal{T})$ given by Eq. (4);
 - 5 $\mathcal{L}_1^{\text{val}} \leftarrow \mathcal{L}_1(\theta_1^*; \mathcal{V})$;
 - 6 $K \leftarrow 1$;
 - 7 **repeat**
 - 8 $K \leftarrow K + 1$;
 - 9 $\theta_K^* \leftarrow \arg \min_{\theta_K} \mathcal{L}_K(\theta_K; \mathcal{T})$ given by (5);
 - 10 $\mathcal{L}_K^{\text{val}} \leftarrow \mathcal{L}_K(\theta_K^*; \mathcal{V})$;
 - 11 **until** $\mathcal{L}_K^{\text{val}} / \mathcal{L}_1^{\text{val}} > \text{tol}$;
 - 12 $d_0 \leftarrow K - 1$;
-

We also consider discrete Hamiltonian lattice systems consisting of N identical nodes, which can potentially be large in number, with dynamic variables $(\mathbf{q}, \mathbf{p}) = (q_1, \dots, q_N, p_1, \dots, p_N) \in \mathbb{R}^{2N}$. While numerous Hamiltonian systems bear a different symplectic structure and a different form of the Hamiltonian, the present form constitutes a large enough class of problems of relevance to applications (as is reflected in the citations below) that merits, in our view, the present investigation. Generalizations to other types of Hamiltonian systems are worthwhile to consider in their own right and are deferred to future work. The systems we examine all have a Hamiltonian function of the following form:

$$H(\mathbf{q}, \mathbf{p}) = T(\mathbf{p}) + V(\mathbf{q}), \quad (10)$$

where $T(\mathbf{p}) = \sum_{n=1}^N \frac{p_n^2}{2}$ represents the kinetic energy, and $V(\mathbf{q})$ denotes the potential energy. We assume periodic boundary conditions, so $q_{N+1} = q_1$. By selecting different forms of the potential $V(\mathbf{q})$, these systems can be either integrable or non-integrable.

- **Discrete sine-Gordon system.** The discrete sine-Gordon system consists of a one-dimensional lattice of particles connected by nonlinear springs [43, 44]. The Hamiltonian for this system is defined as in (10), with a nonlinear potential:

$$V(\mathbf{q}) = \sum_{n=1}^N \left[\frac{C}{2} (q_{n+1} - q_n)^2 + 1 - \cos q_n \right],$$

where C is a small nonlinear coupling parameter. In this model, the above mentioned energy is the only conserved quantity.

- **Calogero-Moser system.** The Calogero-Moser system is a classical mechanics model describing particles that interact via a pairwise potential inversely proportional to the square of their relative distance [28, 27]:

$$V(\mathbf{q}) = \sum_{l < k} \frac{1}{(q_k - q_l)^2}$$

This system is fully integrable, meaning it has N independent conserved quantities that are in involution. These conserved quantities are directly associated with the underlying symmetries of the Hamiltonian [28].

- **Toda lattice.** The Toda lattice [25] models the dynamics of a nonlinear one-dimensional crystal. It describes the motion of a chain of particles interacting through exponential forces that depend on the distance between nearest neighbors. The potential energy of the system is given by:

$$V(\mathbf{q}) = \sum_{n=1}^N [e^{q_n - q_{n-1}} + (q_{n+1} - q_n) - 1] \quad (11)$$

The Toda lattice is also fully integrable, possessing N conservation quantities. These conservation laws are explicitly derived in the classic study by [45].

- **Fermi-Pasta-Ulam-Tsingou system.** Finally, the Fermi-Pasta-Ulam-Tsingou (FPUT) system is closely associated with the Toda lattice [46, 26], resembling a leading order Taylor-expansion thereof. Its nonlinear potential is:

$$V(\mathbf{q}) = \sum_{n=1}^N (q_n - q_{n+1})^2/2 - (q_{n+1} - q_n)^3/6$$

However, unlike the Toda lattice (11), the FPUT system is non-integrable. In addition to conserving the Hamiltonian, the relevant model only conserves the momentum, $P = \sum_{n=1}^N p_n$.

5.1 Data Generation and Hyperparameters

The dataset $\mathcal{D} = \{\mathbf{x}^{(i,j)} = (\mathbf{q}^{(i,j)}, \mathbf{p}^{(i,j)}) : 1 \leq i \leq I, 1 \leq j \leq J\}$ (6) is generated by numerically integrating the systems using the 8th-order Runge-Kutta method [47]. For simplicity, all initial conditions are uniformly sampled from a Euclidean box $[-r, r]^{2d}$. Table 1 lists the parameters used for simulating each system, including:

- I : the number of trajectories.
- J : the number of time steps in each trajectory.
- T : the terminal time of the simulation.
- r : the size of the sampling box.

To learn the Hamiltonian of the system from \mathcal{D} , we first estimate the time-derivative data $\dot{\mathcal{D}} = \{\dot{\mathbf{x}}^{(i,j)} = (\dot{\mathbf{q}}^{(i,j)}, \dot{\mathbf{p}}^{(i,j)}) : 1 \leq i \leq I, 1 \leq j \leq J\}$ using the 8th-order central differences. A seven-layer fully-connected neural network, with 1000 hidden units per layer and tanh activation function,

Physics Systems	I	J	T	r
1d Harmonic Oscillator	200	20	1	10^4
2d Harmonic Oscillator	50	20	2	10^4
Discrete Sine-Gordon	100	50	2	10^4
Calogero-Moser	200	50	2	10^4
Toda lattice	50	50	2	10
FPUT	1500	50	1	50

Table 1: Parameters used for data generation. See Section 5.1 for a detailed description of the notations.

Number of Layers	7
Batch Size	32
Input/Output dimension of Each Layer	1000
Activation Function	\tanh
Initial Learning Rate	1e-5
Scheduled Learning Rate for Fine-Tuning	1e-9
Initial Training Steps	40000
Fine-Tuning Steps	20000
Adam β_1	0.9
Adam β_2	0.999
Adam Weight Decay	0

Table 2: Hyperparameters for training the HNNs

is employed to parameterize the HNN. The network is trained using the Adam optimizer [48] on random batches of size 32. The initial learning rate is set to 10^{-5} and training continues for 40,000 steps, after which the learning rate is reduced to 10^{-9} for an additional 20,000 steps to fine-tune the HNN and ensure convergence. A detailed summary of the hyperparameters is provided in Table 2. Our method is relatively robust to changes in hyperparameters, so slight deviations from the chosen set of values do not lead to qualitatively different final outcomes.

5.2 Results

We carefully examine the errors that can arise when learning a Hamiltonian system through HNN from system trajectories, with a particular focus on the 1D harmonic oscillator. We then further explore how these inaccuracies can impact the downstream neural deflation learning of the remaining conservation laws for the 2D harmonic oscillator and other Hamiltonian lattice systems.

5.2.1 Harmonic Oscillators

1D harmonic oscillator. We first examine the relative error of the HNN-approximated Hamiltonian $H_{\xi^*}(\mathbf{q}, \mathbf{p})$ compared to the ground truth Hamiltonian $H(\mathbf{q}, \mathbf{p})$ (9). Since the neural deflation method relies not on the value of the Hamiltonian itself but on the vector field $f(\mathbf{x}) = (\nabla_{\mathbf{p}}H, -\nabla_{\mathbf{q}}H)$, the relative error is measured by

$$\text{Relative error} = \frac{\|(\nabla_{\mathbf{p}}H_{\xi^*}, -\nabla_{\mathbf{q}}H_{\xi^*}) - (\nabla_{\mathbf{p}}H, -\nabla_{\mathbf{q}}H)\|}{\|(\nabla_{\mathbf{p}}H, -\nabla_{\mathbf{q}}H)\|} \quad (12)$$

Figure 2 visualizes the relative error over the domain $[-10^4, 10^4]$, consistent with the domain used for sampling the training trajectories; see Table 1. The HNN achieves high accuracy, with most relative errors within 10^{-3} , in approximating the true dynamics. This accuracy supports the application of the HNN approach to more complex systems, enhancing confidence in its effectiveness for the downstream neural deflation method.

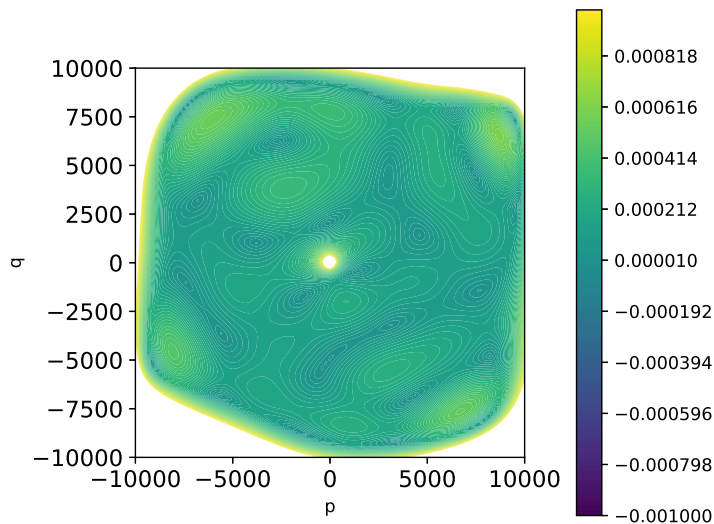


Figure 2: Relative error of HNNs, as defined in Eq. (12), evaluated over the domain $[-10^4, 10^4]$ for the 1D harmonic oscillator.

2D harmonic oscillator. We first train an HNN using data generated from the 2D oscillator system, similar to the 1D case. The learned Hamiltonian is then used as input for the neural deflation method, following Algorithm 1. As part of an ablation study, we also explore the effects of varying deflation strength, using $\alpha = 1.0$ and $\alpha = 0.5$ in Eq. (5).

Figure 3 compares (a) our model, which learns exclusively from system trajectories, with (b) the original neural deflation method [1], which uses additional explicit knowledge of the ground truth differential equation. Both approaches exhibit a sharp increase in the validation loss $\mathcal{L}_k(\theta_k^*; \mathcal{V})$, by several orders of magnitude, at $k = 3$, depending also on the value of the deflation exponent α . This result suggests that both methods have correctly identified the system’s integrability (as indicated in the final step of Algorithm 1) and successfully discovered a maximal set of (two)

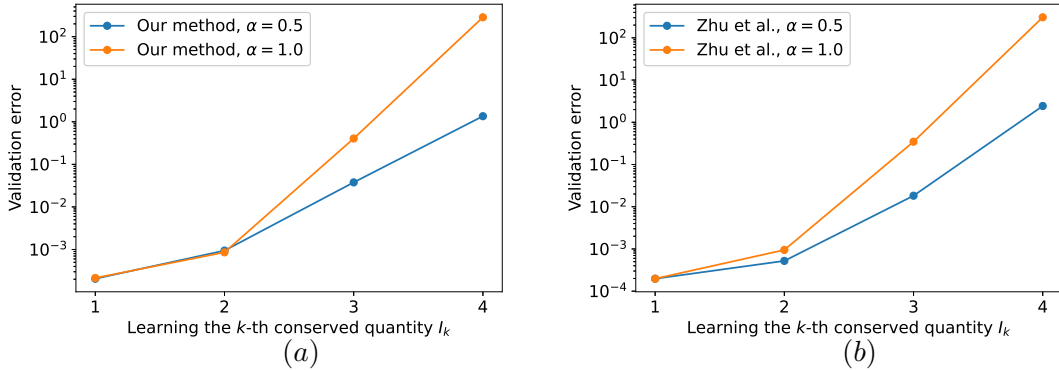


Figure 3: 2D harmonic oscillator. This figure shows the validation losses $\{\mathcal{L}_k(\boldsymbol{\theta}_k^*; \mathcal{V})\}_{k=1}^4$ for the learned conserved quantities $\{I_k(\cdot; \boldsymbol{\theta}_k^*)\}_{k=1}^4$ under different deflation strengths ($\alpha = 1.0$ and $\alpha = 0.5$). Results are compared for: (a) our model, which learns solely from system trajectories, and (b) the original neural deflation method [1], which uses explicit knowledge of the ground truth differential equation. Both methods exhibit a significant increase in loss at $k = 3$, indicating successful identification of the system’s integrability, as per Algorithm 1.

independent conservation laws that are in involution. Given that a larger deflation strength of $\alpha = 1.0$ results in a more pronounced jump in loss, we will use this value of α for the remaining examples.

5.2.2 Discrete Sine-Gordon System

Figure 4 offers a side-by-side comparison of our model with the original neural deflation method [1] applied to the non-integrable discrete sine-Gordon system, with the number of lattice sites (and thus the degrees of freedom) set to $N = 6 = d$. The results are similar, despite our model relying solely on simulated system trajectories. Both methods exhibit a significant increase in validation loss at $k = 2$, by about 2 orders of magnitude, consistent with the fact that the underlying system has only one independent conservation law (refer to the last line of Algorithm 1).

5.2.3 Calogero-Moser System

Figure 5 presents the results when the methods are applied to the fully integrable Calogero-Moser system with $N = 6$ lattice sites. At first glance, our method [panel (a)] achieves comparable, if not superior, performance compared to the original neural deflation method [panel (b)]. Both methods exhibit a significant jump in test loss precisely at $k = 7$, indicating the successful learning of six independent, Poisson-commuting conservation laws in this integrable system with six degrees of freedom. Notably, the jump in test loss is even more pronounced with our method compared to the original neural deflation approach.

However, a closer examination of the Hamiltonian learned by the HNN reveals some unexpected behavior. Due to the short-range interactions in the Calogero-Moser system, which are governed by an inverse cubic force, most particles maintain constant speeds and only exchange momentum

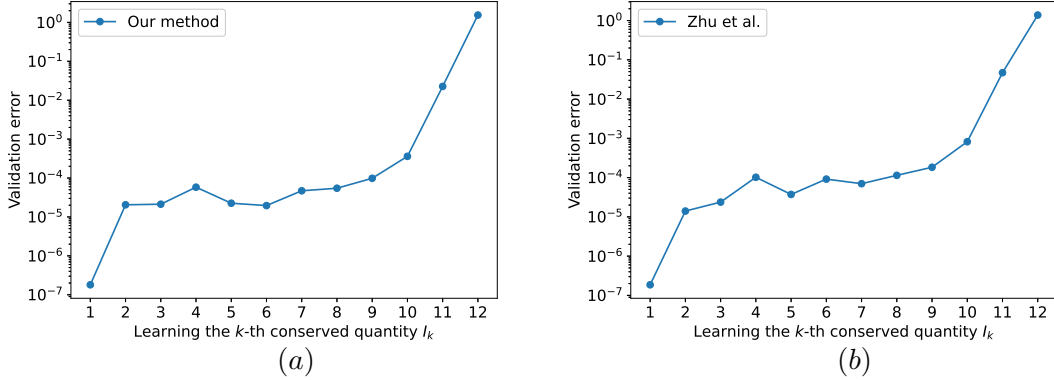


Figure 4: Discrete sine-Gordon system with the number of lattice sites/degrees of freedom $N = d = 6$. This figure shows the validation losses $\{\mathcal{L}_k(\boldsymbol{\theta}_k^*; \mathcal{V})\}_{k=1}^{2d}$ for the learned conserved quantities $\{I_k(\cdot; \boldsymbol{\theta}_k^*)\}_{k=1}^{2d}$. Results are compared for: (a) our model, which learns solely from system trajectories, and (b) the original neural deflation method [1], which uses explicit knowledge of the ground truth differential equation. Both methods exhibit a significant increase in loss at $k = 2$, consistent with the fact that the underlying system has only *one* independent conservation law; see Algorithm 1.

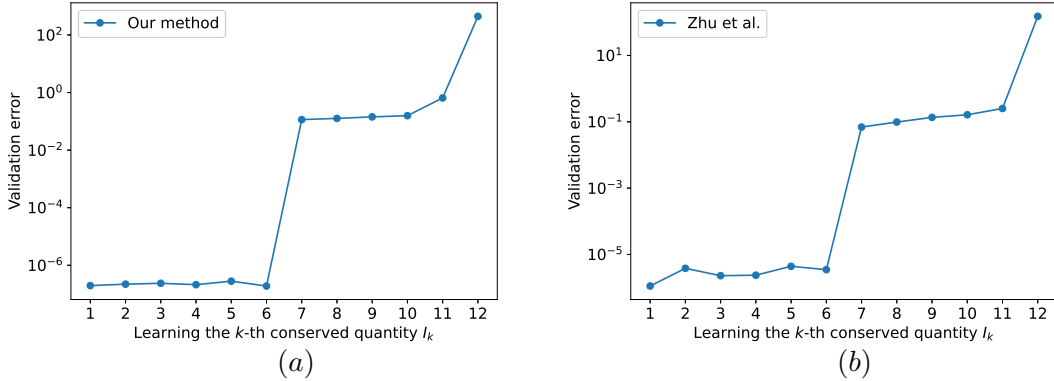


Figure 5: Calogero-Moser system with the number of lattice sites/degrees of freedom $N = d = 6$. This figure shows the validation losses $\{\mathcal{L}_k(\boldsymbol{\theta}_k^*; \mathcal{V})\}_{k=1}^{2d}$ for the learned conserved quantities $\{I_k(\cdot; \boldsymbol{\theta}_k^*)\}_{k=1}^{2d}$. Results are compared for: (a) our model, which learns solely from system trajectories, and (b) the original neural deflation method [1], which uses explicit knowledge of the ground truth differential equation. Both methods **appear** to exhibit a significant increase in loss at $k = 7$, consistent with the fact that the underlying system is fully-integrable.

almost instantaneously during brief collisions (i.e., when $q_i \approx q_j$). This phenomenon is illustrated in Figure 6, where the (rare) momentum exchange is indicated by the sudden change of colors in the columns for p_i . As a result, the time-derivative data $\dot{\mathcal{D}}$, obtained using finite differences, makes the system behave similarly to one with zero potential, with rare “outliers” occurring during particle collisions. Consequently, the HNN tends to approximate the system Hamiltonian

as having zero potential energy.

	q_1	q_2	q_3	p_1	p_2	p_3
55.2901	166.947	130.794	39.2806	-66.8154	127.683	
56.0757	165.611	133.348	39.2806	-66.8154	127.683	
56.8614	164.275	135.902	39.2806	-66.8154	127.683	
57.647	162.938	138.455	39.2806	-66.8154	127.683	
67.8599	171.653	145.566	39.2806	127.683	-66.8154	
68.6455	174.207	144.23	39.2806	127.683	-66.8154	
69.4311	176.76	142.894	39.2806	127.683	-66.8154	
70.2168	179.314	141.557	39.2806	127.683	-66.8154	
71.0024	181.867	140.221	39.2806	127.683	-66.8154	
71.788	184.421	138.885	39.2806	127.683	-66.8153	
72.5736	186.975	137.549	39.2806	127.683	-66.8153	
...						
88.1052	281.46	101.641	-66.8153	127.683	39.2806	
86.7689	284.014	102.427	-66.8153	127.683	39.2806	
85.4326	286.567	103.212	-66.8153	127.683	39.2806	
84.0963	289.121	103.998	-66.8153	127.683	39.2806	
82.7599	291.675	104.784	-66.8153	127.683	39.2806	

Figure 6: A simulated trajectory from the Calogero-Moser system with $N = d = 3$ degrees of freedom. Each column presents the time evolution of the dynamic variables q_i and p_i . The particles move at constant speeds, exchanging momentum almost instantaneously during collisions (when $q_i \approx q_j$), due to short-range interactions governed by an inverse cubic force. This momentum exchange is indicated by the sudden change of colors in the columns for p_i . To highlight the moments of momentum exchange, some time data has been omitted from the illustration.

A potential solution to this issue is to use neural ODEs [49] instead of HNNs to learn the underlying Hamiltonian, thus avoiding the inaccuracies introduced by finite difference estimation of time derivatives. This approach will be explored in future work.

5.2.4 Toda system

We now examine the integrable Toda system with degrees of freedom $d = N = 6$, as illustrated in Figure 7. Similar to the original neural deflation method shown in panel (b), our method in panel (a) exhibits a significant increase in validation loss at $k = 7$, indicating the successful identification of $d_0 = 7 - 1 = 6$ independent conservation laws in involution, thereby confirming the system’s integrability. However, the jump in validation loss is more pronounced in the original neural deflation method [1], which explicitly incorporates the Hamiltonian into the algorithm. This discrepancy likely arises from the exponential term in the Toda lattice potential (11), which complicates the high-accuracy approximation of the Hamiltonian by HNN over a large domain. Nevertheless, the similarity in loss behavior between our data-driven method, which learns conservation laws from system trajectories, and the original neural deflation method, which assumes explicit knowledge of the underlying ODE system, highlights the potential of our approach for learning conservation laws and assessing system integrability from observed trajectories.

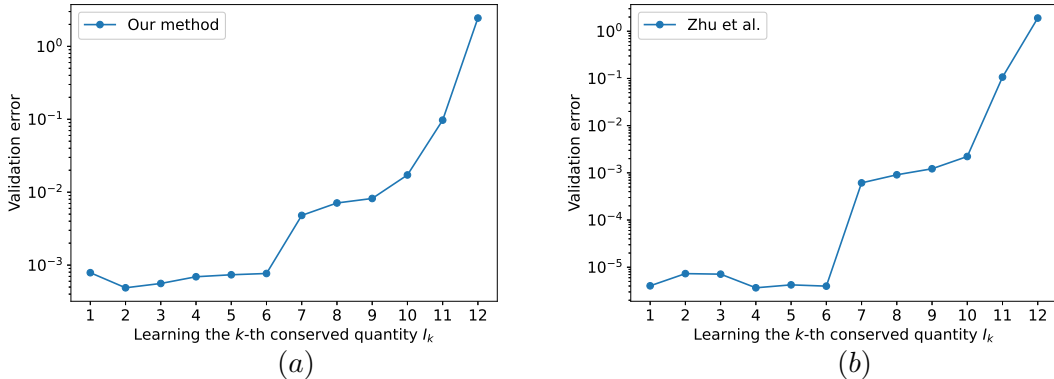


Figure 7: Toda system with the number of lattice sites/degrees of freedom $N = d = 6$. This figure shows the validation losses $\{\mathcal{L}_k(\boldsymbol{\theta}_k^*; \mathcal{V})\}_{k=1}^{2d}$ for the learned conserved quantities $\{I_k(\cdot; \boldsymbol{\theta}_k^*)\}_{k=1}^{2d}$. Results are compared for: (a) our model, which learns solely from system trajectories, and (b) the original neural deflation method [1], which uses explicit knowledge of the ground truth differential equation. Both methods show a notable increase in validation loss at $k = 7$, indicating the successful identification of $d_0 = 7 - 1 = 6$ independent conservation laws in involution, thereby confirming the integrability of the Toda system. The jump in validation loss is more pronounced in panel (b), where the original neural deflation method incorporates explicit information about the underlying Hamiltonian [1]. The reduced sharpness of the loss jump in our model likely stems from the exponential term in the Toda system’s potential 11, which complicates accurate learning of the Hamiltonian.

5.2.5 FPUT System

Finally, we turn to the non-integrable FPUT system with the number of degrees of freedom remaining $d = N = 6$, as illustrated in Figure 8. Similar to the original neural deflation method in panel (b), our approach in panel (a) shows a clear increase in validation loss after identifying the first conservation law, indicating the non-integrable nature of the system. Unlike the Toda system, where the jump in validation loss differed significantly between methods (see Section 5.2.4), the increase here is of comparable magnitude. This is likely because the polynomial potential in the FPUT system is much easier for the HNN to approximate accurately. However, consistent with [1], our method only detects one conservation law, even though the FPUT system has two independent conservation laws in involution (momentum and Hamiltonian). It remains an open question whether a modified neural deflation method could correctly identify both. Despite this, the comparable validation loss patterns between our method and the original neural deflation approach suggest that our method shows strong potential for effectively learning conservation laws and evaluating system integrability using only trajectory data.

6 Conclusions and Future Works

In this work, we introduced a data-driven method for discovering independent conservation laws in Hamiltonian systems using neural deflation, relying solely on system trajectory data. Our

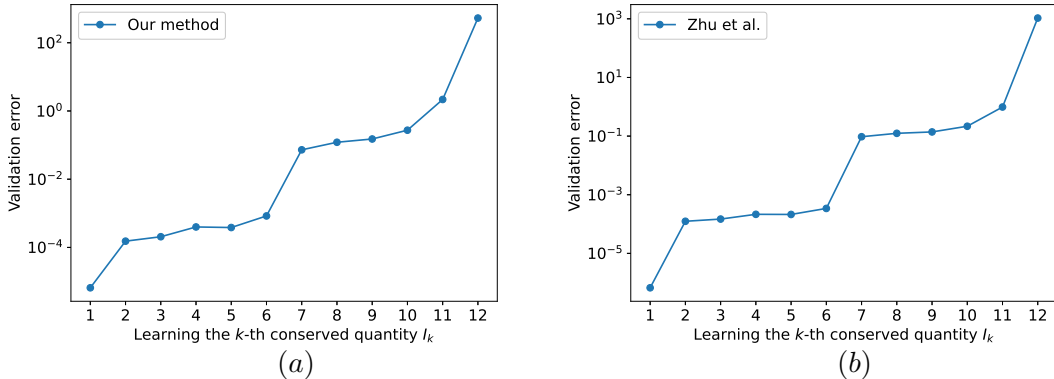


Figure 8: FPUT system with the number of lattice sites/degrees of freedom $N = d = 6$. This figure shows the validation losses $\{\mathcal{L}_k(\boldsymbol{\theta}_k^*; \mathcal{V})\}_{k=1}^{2d}$ for the learned conserved quantities $\{I_k(\cdot; \boldsymbol{\theta}_k^*)\}_{k=1}^{2d}$. Results are compared for: (a) our model, which learns solely from system trajectories, and (b) the original neural deflation method [1], which uses explicit knowledge of the ground truth differential equation. Both methods exhibit a significant increase in loss at $k = 2$, indicating the non-integrability nature of the FPUT system. See Section 5.2.5 for a detailed discussion of this result.

method successfully identified the (almost) exact number of conservation laws in both integrable and non-integrable systems, demonstrating performance comparable to prior state-of-the-art approaches that require explicit knowledge of the underlying ODEs. These results underscore the potential of our approach for learning conservation laws from directly observed data that may, in principle, arise even from a physical experiment.

A promising focal point for future work consists of improving the accuracy of data-driven Hamiltonian learning for systems with complex dynamics, such as the Toda and Calogero-Moser systems. In particular, in the Calogero-Moser system, short-range interactions cause particles to maintain constant speeds, with momentum exchanges occurring only during brief collisions (in a way reminiscent of hard sphere models), making finite difference estimates of time derivatives unreliable. To address this, a promising avenue involves exploring neural ODEs in place of HNNs, which can avoid errors from finite differences and remove the need for short time intervals in trajectory data. On the other hand, it is also an open problem whether the momentum conservation of FPUT models can be identified in the context of the methods proposed herein. Additionally, we plan to use symbolic regression to connect the learned conservation laws to known physical quantities or those identified through integrability techniques, enhancing interpretability. There exist also interesting perspectives regarding connecting Liouville with other types of integrability (e.g., Frobenius) [21], as well as in connection to identifying the symplectic transformations leading to the action-angle variables associated with the conserved quantities [23]. These directions are currently under investigation and will be detailed in future work.

Acknowledgements

This material is based upon work supported by the U.S. National Science Foundation under awards DMS-2052525, DMS-2140982, DMS-2244976 (WZ), PHY-2110030, PHY-2408988, and DMS-2204702 (PGK), as well as DMS-2220211 (HZ). Additional support was provided by the Simons Foundation Collaboration Grants for Mathematicians 706383 (HZ).

References

- [1] Wei Zhu, Hong-Kun Zhang, and P. G. Kevrekidis. Machine learning of independent conservation laws through neural deflation. *Phys. Rev. E*, 108:L022301, Aug 2023.
- [2] A. Goriely. *Integrability and Nonintegrability of Dynamical Systems*. Advanced series in nonlinear dynamics. World Scientific, 2001.
- [3] Yuri S Kivshar and Govind P Agrawal. *Optical solitons: from fibers to photonic crystals*. Academic press, 2003.
- [4] S. Stringari and L.P. Pitaevskii. *Bose-Einstein Condensation*. Oxford University Press, Oxford, United Kingdom, 2003.
- [5] T. Dauxois and M. Peyrard. *Physics of Solitons*. Cambridge University Press, 1st edition, 2006.
- [6] E. Infeld and G. Rowlands. *Nonlinear Waves, Solitons and Chaos*. Cambridge University Press, Cambridge, UK, 1990.
- [7] M. Kono and M. Škorić. *Nonlinear Physics of Plasmas*. Springer-Verlag, Heidelberg, 2010.
- [8] M.J. Ablowitz. *Nonlinear Dispersive Waves, Asymptotic Analysis and Solitons*. Cambridge University Press, Cambridge, 2011.
- [9] Ruoxia Yao, Changzheng Qu, and Zhibin Li. Painlevé property and conservation laws of multi-component mKdV equations. *Chaos, Solitons and Fractals*, 22(3):723–730, 2004.
- [10] R. Conte. *The Painlevé property*. Springer-Verlag, New York, 1999.
- [11] Giancarlo Benettin, Luigi Galgani, Antonio Giorgilli, and Jean-Marie Strelcyn. Lyapunov characteristic exponents for smooth dynamical systems and for Hamiltonian systems; a method for computing all of them. Part 1: Theory. *Meccanica*, 15(1):9–20, 1980.
- [12] G Benettin, L Galgani, A Giorgilli, and JM Strelcyn. Lyapunov characteristic exponents for smooth dynamical systems; a method for computing all of them. Part 2: Numerical application. *Meccanica*, 15:21–30, 1980.
- [13] Thudiyangal Mithun, Aleksandra Maluckov, Ana Mančić, Avinash Khare, and Panayotis G. Kevrekidis. How close are integrable and nonintegrable models: A parametric case study based on the salerno model. *Phys. Rev. E*, 107:024202, Feb 2023.
- [14] Bernard O Koopman. Hamiltonian systems and transformation in hilbert space. *Proceedings of the National Academy of Sciences*, 17(5):315–318, 1931.
- [15] Igor Mezić. Spectral properties of dynamical systems, model reduction and decompositions. *Nonlinear Dynamics*, 41:309–325, 2005.
- [16] Eurika Kaiser, J Nathan Kutz, and Steven L Brunton. Discovering conservation laws from data for control. In *2018 IEEE Conference on Decision and Control (CDC)*, pages 6415–6421. IEEE, 2018.

- [17] Sebastian J. Wetzel, Roger G. Melko, Joseph Scott, Maysum Panju, and Vijay Ganesh. Discovering symmetry invariants and conserved quantities by interpreting siamese neural networks. *Phys. Rev. Res.*, 2:033499, Sep 2020.
- [18] Ziming Liu and Max Tegmark. Machine learning conservation laws from trajectories. *Phys. Rev. Lett.*, 126:180604, May 2021.
- [19] Shivam Arora, Alex Bihlo, Rüdiger Brecht, and Pavel Holba. Model-agnostic machine learning of conservation laws from data. *arXiv preprint arXiv:2301.07503*, 2023.
- [20] Peter Y Lu, Rumen Dangovski, and Marin Soljačić. Discovering conservation laws using optimal transport and manifold learning. *Nature Communications*, 14(1):4744, 2023.
- [21] Ziming Liu, Varun Madhavan, and Max Tegmark. Machine learning conservation laws from differential equations. *Physical Review E*, 106(4):045307, 2022.
- [22] Ziming Liu, Patrick Obin Sturm, Saketh Bharadwaj, Sam J Silva, and Max Tegmark. Interpretable conservation laws as sparse invariants. *Physical Review E*, 109(2):L023301, 2024.
- [23] Roberto Bondesan and Austen Lamacraft. Learning symmetries of classical integrable systems. *arXiv preprint arXiv:1906.04645*, 2019.
- [24] Seungwoong Ha and Hawoong Jeong. Discovering invariants via machine learning. *Physical Review Research*, 3(4):L042035, 2021.
- [25] M. Toda. *Theory of Nonlinear Lattices*. Ergebnisse der Mathematik Und Ihrer Grenzgebiete. Springer-Verlag, 1989.
- [26] G. Gallavotti. *The Fermi-Pasta-Ulam Problem: A Status Report*. Lecture Notes in Physics. Springer Berlin Heidelberg, 2007.
- [27] F. Calogero. Solution of the One-Dimensional N-Body Problems with Quadratic and/or Inversely Quadratic Pair Potentials. *Journal of Mathematical Physics*, 12(3):419–436, 03 1971.
- [28] J Moser. Three integrable hamiltonian systems connected with isospectral deformations. *Advances in Mathematics*, 16(2):197–220, 1975.
- [29] Sebastian J. Wetzel, Roger G. Melko, Joseph Scott, Maysum Panju, and Vijay Ganesh. Discovering symmetry invariants and conserved quantities by interpreting siamese neural networks. *Phys. Rev. Res.*, 2:033499, Sep 2020.
- [30] Vladimir Igorevich Arnol'd. *Mathematical methods of classical mechanics*, volume 60. Springer Science & Business Media, 2013.
- [31] P. E. Farrell, Á. Birkisson, and S. W. Funke. Deflation techniques for finding distinct solutions of nonlinear partial differential equations. *SIAM Journal on Scientific Computing*, 37(4):A2026–A2045, 2015.

- [32] Peter Toth, Danilo Jimenez Rezende, Andrew Jaegle, Sébastien Racanière, Aleksandar Botev, and Irina Higgins. Hamiltonian generative networks. *arXiv preprint arXiv:1909.13789*, 2019.
- [33] Tom Bertalan, Felix Dietrich, Igor Mezić, and Ioannis G Kevrekidis. On learning hamiltonian systems from data. *Chaos: An Interdisciplinary Journal of Nonlinear Science*, 29(12), 2019.
- [34] Sam Greydanus, Misko Dzamba, and Jason Yosinski. Hamiltonian neural networks. In *NeurIPS*, page 15379–15389, 2019.
- [35] Chen-Di Han, Bryan Glaz, Mulugeta Haile, and Ying-Cheng Lai. Adaptable hamiltonian neural networks. *Phys. Rev. Res.*, 3:023156, May 2021.
- [36] Rishabh Gupta, Raja Selvarajan, Manas Sajjan, Raphael D Levine, and Sabre Kais. Hamiltonian learning from time dynamics using variational algorithms. *The Journal of Physical Chemistry A*, 127(14):3246–3255, 2023.
- [37] Marios Mattheakis, David Sondak, Akshunna S Dogra, and Pavlos Protopapas. Hamiltonian neural networks for solving equations of motion. *Physical Review E*, 105(6):065305, 2022.
- [38] Przemyslaw Bienias, Alireza Seif, and Mohammad Hafezi. Meta hamiltonian learning. *arXiv preprint arXiv:2104.04453*, 2021.
- [39] Marco David and Florian Méhats. Symplectic learning for hamiltonian neural networks. *Journal of Computational Physics*, 494:112495, 2023.
- [40] Zhengdao Chen, Jianyu Zhang, Martin Arjovsky, and Léon Bottou. Symplectic recurrent neural networks. *arXiv preprint arXiv:1909.13334*, 2019.
- [41] Daniel DiPietro, Shiyong Xiong, and Bo Zhu. Sparse symplectically integrated neural networks. *Advances in Neural Information Processing Systems*, 33:6074–6085, 2020.
- [42] Katsiaryna Haitsiukevich and Alexander Ilin. Learning trajectories of hamiltonian systems with neural networks. In *International Conference on Artificial Neural Networks*, pages 562–573. Springer, 2022.
- [43] O. M. Braun and Y. S. Kivshar. *The Frenkel-Kontorova model: concepts, methods and applications*. Texts and monographs in physics. Springer-Verlag, Berlin Heidelberg, 2004.
- [44] Jesús Cuevas-Maraver, Panayotis Kevrekidis, and Floyd Williams. *The sine-Gordon Model and its Applications: From Pendula and Josephson Junctions to Gravity and High-Energy Physics*. 01 2014.
- [45] M. Hénon. Integrals of the toda lattice. *Phys. Rev. B*, 9:1921–1923, Feb 1974.
- [46] E. Fermi, P Pasta, S Ulam, and M Tsingou. Studies of the nonlinear problems. 5 1955.
- [47] Ernst Hairer, Syvert Norsett, and Gerhard Wanner. *Solving Ordinary Differential Equations I: Nonstiff Problems*, volume 8. 01 1993.
- [48] Diederik Kingma and Jimmy Ba. Adam: A method for stochastic optimization. In *ICLR*, 12 2014.

- [49] Ricky TQ Chen, Yulia Rubanova, Jesse Bettencourt, and David K Duvenaud. Neural ordinary differential equations. In *NeurIPS*, volume 31, 2018.